Hydrodynamical study of neutrino-driven wind as an r-process site

K. Sumiyoshi[a,1], H. Suzuki[b], K. Otsuki[c], M. Terasawa[a,c,d], and S. Yamada[d]

[a]The Institute of Physical and Chemical Research (RIKEN),

Hirosawa, Wako, Saitama 351-0198, Japan

[b]High Energy Accelerator Research Organization (KEK),

Oho, Tsukuba, Ibaraki 305-0801, Japan

[c]National Astronomical Observatory (NAO),

Oosawa, Mitaka, Tokyo 181-8588, Japan

[d]Department of Physics, School of Science, The University of Tokyo,

Hongo, Bunkyo, Tokyo 113-0033, Japan

[1]e-mail: sumi@postman.riken.go.jp

Abstract

We study the neutrino-driven wind from the proto-neutron star by the general relativistic hydrodynamical simulations. We examine the properties of the neutrino-driven wind to explore the possibility of the r-process nucleosynthesis. The numerical simulations with the neutrino heating and cooling processes are performed with the assumption of the constant neutrino luminosity by using realistic profiles of the proto-neutron star (PNS) as well as simplified models. The dependence on the mass of PNS and the neutrino luminosity is studied systematically. Comparisons with the analytic treatment in the previous studies are also done. In the cases with the realistic PNS, we found that the entropy per baryon and the expansion time scale are neither high nor short enough for the r-process within the current assumptions. On the other hand, we found that the expansion time scale obtained by the hydrodynamical simulations is systematically shorter than that in the analytic solutions due to our proper treatment of the equation of state. This fact might lead to the increase of the neutron-to-seed ratio, which is suitable for the r-process in the neutrino-driven wind. Indeed, in the case of massive and compact proto-neutron stars with high neutrino luminosities, the expansion time scale is found short enough in the hydrodynamical simulations and the r-process elements up to $A \sim 200$ are produced in the r-process network calculation.

1 Introduction

Finding the origin of heavy elements has been an attractive and longstanding issue in astrophysics. Among various nucleosynthesis processes, the rapid neutron capture process (r-process) is believed to be essential to create many of heavy elements (Burbidge et al. 1957). Since the r-process nucleosynthesis requires enough neutron source to create heavy elements up to $A \sim 200$, how and where, in the Universe, the condition for the r-process is realized has been a central issue. The recent observations of r-process elements in metal poor stars (Sneden et al. 1996) further strengthen the motivation to identify the r-process site(s) in the Universe.

Among various proposed sites, the type II supernovae have been focused as the most plausible site and many studies have been made to find out where exactly the r-process occurs during the event of supernova explosions (Hillebrandt 1978; Cowan, Thielemann & Truran 1991). The neutrino-driven wind from a proto-neutron star, just born in the supernova explosion, has been suggested as a promising site (Meyer et al. 1992; Woosley et al. 1994). The surface material of the proto-neutron star is heated by the supernova neutrinos and a portion of the material is ejected as a hot bubble having a high entropy per baryon ($\sim 400 k_B$). Due to this high entropy, the neutron-to-seed ratio after the charged particle reactions freeze out (α-rich freeze-out) becomes high enough to lead to the r-process nucleosynthesis.

The dynamics of the neutrino-driven wind and its outcome of the nucleosynthesis have been studied since then (Qian & Woosley 1996 (here after QW); Hoffman, Woosley & Qian 1997; Otsuki 1999, Otsuki et al. 1999). Qian and Woosley have investigated the dynamics of the neutrino-driven wind both by analytic treatments and numerical simulations. They have shown that the entropy per baryon in the wind turns out too low by a factor of $2-3$ for the r-process. Witti et al. (1994) and Takahashi et al. (1994) have performed the numerical simulations of the neutrino-driven wind and the r-process adopting an initial configuration provided by Wilson. The entropy per baryon in their simulation falls again short for the r-process. They had to introduce artificially an extra factor to scale down the densities along the trajectory to get high entropies for successful r-process. These studies, which are mostly done non-relativistically, have cast questions on the scenario of high entropy bubble for the r-process.

Cardall and Fuller (1997) have further studied the general relativistic dynamics of the

neutrino-driven wind with the analytic treatment. They have shown that the general relativistic effects increase the entropy and shorten the expansion time scale and will be favorable for the r-process. Furthermore, Otsuki et al. (1999) have shown with extensive parametric studies that the r-process is actually possible in the neutrino-driven wind with a short expansion time scale even if the entropy is not as high as $\sim 400k_B$. They have demonstrated by the network calculation that the r-process up to $A \sim 200$ can take place for massive and compact neutron stars having high neutrino luminosities. These general relativistic studies revive some interests in the neutrino-driven wind as an r-process site and suggest that detailed studies are necessary with general relativity for realistic models of proto-neutron stars and supernova neutrinos.

General relativistic studies have been done so far only analytically for stationary neutrino-driven winds with given mass and radius of the proto-neutron stars. To remove these restrictions, we have performed general relativistic hydrodynamical simulations of the neutrino-driven wind. We have adopted the general relativistic, implicit and Lagrangian hydro code, which were developed for the supernova simulations (Yamada 1997), and have implemented necessary neutrino processes. We aim to perform simulations of the time evolution of the neutrino-driven wind adopting the results of proto-neutron star cooling simulations (Suzuki 1994; Sumiyoshi, Suzuki & Toki 1995). The final goal is to find out whether the r-process takes place in a realistic situation under the general relativistic hydrodynamics and to answer whether the high entropy bubble scenario or the rapid expansion scenario or any other way is realized to create the r-process elements.

In the current paper, we report the first step of this line of research. We adopt the realistic profiles of the proto-neutron stars, but we take rather simple assumptions about the neutrino luminosities and spectra in order to compare with the previous analytic studies. We remark that the relativistic EOS table, which has been completed for supernova simulations (Shen et al. 1998; Shen et al. 1998), enabled us to construct the initial configurations of the wind consistently with the proto-neutron star cooling simulations using the same physical EOS table. We examine systematically the dependence on the mass of proto-neutron stars and the neutrino luminosities.

The paper is arranged as follows. In section 2, after the brief description of the neutrino-

driven wind, we give explanations of our numerical treatment. In section 3, we show the numerical results of simulations for the realistic profiles of the proto-neutron stars (§ 3.1) and the simplified models with given mass and radius (§ 3.2). In section 4, we discuss the r-process condition derived from the numerical simulations (§ 4.1) and describe the r-process network calculation using the trajectory of our simulation (§ 4.2). We demonstrate the case of successful r-process nucleosynthesis from our results. The summary will be given in section 5.

2 Hydrodynamical simulation

The neutrino-driven wind is the mass ejection from the surface of the proto-neutron star due to neutrino heating (Duncan, Shapiro & Wasserman 1986). Since the proto-neutron star, which is formed in the collapse-driven supernova explosion, emits a plenty of neutrinos, a small portion of the surface material might be heated up and ejected by gaining the energy to escape the gravitational potential of the compact object. Ejected matter is expanded and then cools down to the temperature regime for the nucleosynthesis.

The main interest here is the thermodynamical history of ejecta determined by hydrodynamics during the time of the nucleosynthesis. If it is favorable to make the neutron-to-seed ratio high enough during the charged particle reactions, the r-process may take place afterwards. The key quantities are the electron fraction, Y_e, the entropy per baryon, S, and the expansion time scale, τ_{dyn}. A low electron fraction, a high entropy per baryon and a short expansion time scale are known to be favorable for the r-process (Meyer & Brown 1997). We investigate those conditions by performing the hydrodynamical simulations for the surface layers of proto-neutron stars.

2.1 Numerical code

We employ the implicit numerical code for the general relativistic and spherically symmetric hydrodynamics (Yamada 1997). The general relativity is essential here since it is known to influence the properties of neutrino-driven wind and may lead to a better condition for the r-process (Cardall & Fuller, 1997; Otsuki et al. 1999). The implicit time differencing is advan-

tageous to follow the hydrodynamics for a long time compared with the sound crossing time of the numerical mesh. The hydro code uses a Lagrangian mesh, which is suitable to follow the thermal history for the nucleosynthesis. We employ the baryon mass meshes with equal spacing. The grid size ranges typically from $10^{-8}M_\odot$ to $10^{-6}M_\odot$, depending mainly on the luminosity, so as to have enough resolutions.

The heating and cooling processes due to neutrinos are added on top of the hydro code. The optically thin-limit is assumed for neutrinos since the surface region of interest has low densities and is transparent to neutrinos. Although the Boltzmann solver of neutrino transfer is already implemented in the numerical code (Yamada, Janka & Suzuki 1999), we do not solve the Boltzmann equation, but instead we set the neutrino distribution function at each Lagrangian mesh point as described below.

We treat the following neutrino reactions as sources of heating and cooling,

$$\nu_e + n \leftrightarrow e^- + p, \tag{1}$$

$$\bar{\nu}_e + p \leftrightarrow e^+ + n, \tag{2}$$

$$\nu_i + e^- \leftrightarrow \nu_i + e^-, \tag{3}$$

$$\nu_i + e^+ \leftrightarrow \nu_i + e^+, \tag{4}$$

$$\bar{\nu}_i + e^- \leftrightarrow \bar{\nu}_i + e^-, \tag{5}$$

$$\bar{\nu}_i + e^+ \leftrightarrow \bar{\nu}_i + e^+, \tag{6}$$

$$\nu_i + \bar{\nu}_i \leftrightarrow e^- + e^+, \tag{7}$$

where the index i of ν_i stands for neutrino flavors ($i = e, \mu, \tau$). The evaluation of the reaction rates (1) and (2) follows the standard procedure as used in supernova calculations (Yamada, Janka & Suzuki 1999). The heating and cooling rates are calculated by the energy integrals using the distribution functions of neutrinos and electrons in the Boltzmann solver. The Pauli blocking effects for electrons and positrons, the neutron-proton mass difference are thus properly taken into account. This is in contrast to the approximate treatment in QW where the radiation dominated situation is assumed. The other heating and cooling rates due to the pair process and the electron scattering are evaluated by Eqs. (12), (13) and (14) of QW. The evolution of the electron fraction, Y_e, is solved together with hydrodynamics using the collision terms for

the reactions (1) and (2) of the Boltzmann solver (Yamada 1997).

As for the equation of state (EOS) of dense matter, we adopt the table of the relativistic EOS, which is recently derived for supernova simulations (Shen et al. 1998, Shen et al. 1998) in the relativistic nuclear many body framework. It reproduces the nuclear matter saturation and the properties of stable and unstable nuclei in the nuclear chart (Sugahara & Toki 1994; Sumiyoshi, Kuwabara & Toki 1995). The table covers the wide range of density ($10^{5.1} \sim 10^{15.4}$ g/cm^3), electron fraction ($0.0 \sim 0.56$), and temperature ($0 \sim 100$ MeV), which is required for supernova simulations. The electron/positron and photon contributions as non-interacting particles are added to the nuclear contribution of the EOS. The arbitrary degeneracy of electrons and disappearance of positrons at low temperatures are properly treated.

We extend the EOS table toward lower densities below 10^5 g/cm^3 in the current study. Since this low density regime appears in the simulations at temperature below 0.5 MeV, we assume the mixture of neutrons, protons and α-particles in nuclear statistical equilibrium. This is a good approximation at the time of α-rich freeze-out because only a slight amount of nuclei is synthesized. To determine the composition precisely in this temperature regime, one has to solve the nuclear reaction network with the hydrodynamics at the same time. This is a formidable task beyond the current scope of study. We note, however, that the evolution of the electron fraction is properly coupled to hydrodynamics.

As for the neutrino spectra, we take rather simple assumptions in the current study. The neutrino distribution, $f_{\nu_i}(R_{\nu_i})$, at the neutrinosphere is assumed to be monochromatic in energy and isotropic in angle as follows

$$f_{\nu_i}(R_{\nu_i}) = f_{\nu_{i0}} \delta(E_{\nu_i} - \langle E_{\nu_i} \rangle). \tag{8}$$

The coefficient, $f_{\nu_{i0}}$, is determined by the neutrino luminosity, L_{ν_i}, and the radius of the neutrinosphere, R_{ν_i}, as

$$f_{\nu_{i0}} = \frac{2\pi L_{\nu_i}}{\langle E_{\nu_i} \rangle^3 R_{\nu_i}^2}, \tag{9}$$

where the average energy, $\langle E_{\nu_i} \rangle$, L_{ν_i} and R_{ν_i} are given as model parameters. The number density of neutrinos, n_{ν_i}, at radius, r, is given by

$$n_{\nu_i} = \frac{1-x}{4\pi^2} \langle E_{\nu_i} \rangle^2 f_{\nu_{i0}} \tag{10}$$

$$= \frac{1-x}{2\pi}\frac{L_{\nu_i}}{\langle E_{\nu_i}\rangle R_{\nu_i}^2}, \tag{11}$$

where x is defined as

$$x = \left(1 - \frac{R_{\nu_i}^2}{r^2}\right)^{\frac{1}{2}}, \tag{12}$$

to take into account the solid angle subtended by the neutrinosphere (QW). Using this expression of the number density, we set the neutrino distribution at radius, r, as

$$f_{\nu_i}(r) = f_{\nu_{ir}}\delta(E_{\nu_i} - \langle E_{\nu_i}\rangle), \tag{13}$$

where the coefficient, $f_{\nu_{ir}}$, is given by

$$f_{\nu_{ir}} = \frac{2\pi(1-x)L_{\nu_i}}{\langle E_{\nu_i}\rangle^3 R_{\nu_i}^2}. \tag{14}$$

The positions of the neutrinospheres are assumed to be common to all neutrino species in the current study. The general relativistic effects such as the red-shift and the ray bending are not taken into account here. The above approximation for neutrino spectra is just intended to compare with the previous analytic studies. More realistic neutrino spectra will be incorporated in the forthcoming paper.

As for the inner boundary condition, the radius, the gravitational mass and the baryon mass are given. Thermodynamical quantities are set to be the same as those at the innermost mesh point. We adopt the reflecting condition for the velocity. As for the outer boundary, we impose a constant pressure. The thermodynamical quantities are again assumed to be the same as those at the neighboring mesh point inside.

2.2 Initial models

The initial models are constructed based on the hydrostatic configuration of the proto-neutron stars. We take a surface layer of the proto-neutron star and remap it to the hydro code as an initial configuration. We construct initial models in two ways. One is based on the numerical results of the proto-neutron star cooling (Sumiyoshi, Suzuki & Toki 1995) as realistic models. In the second case, we choose the neutron star mass and radius at the inner boundary arbitrarily.

As for the former case, the numerical simulations have been performed by solving the quasi-static evolution of the proto-neutron star with neutrino transport using the multi-energy-group

flux-limited diffusion scheme (Suzuki 1994). In these simulations, we have used the relativistic EOS table, which is the same as the one used in the current study. By so doing, mapping of thermodynamical quantities to the hydro code is done consistently. We choose the cases of the baryon mass of $1.62M_\odot$ and $2.00M_\odot$. Snapshots of density, electron fraction and temperature at a certain time of the proto-neutron star cooling simulations are picked up to be used as initial inputs for the neutrino-driven wind simulations. We remark that the proto-neutron star cooling simulations start from the initial profile provided by Mayle and Wilson, which corresponds to the supernova core at 0.4 seconds after the core bounce. We cut out the surface layer containing a small baryon mass (typically from $10^{-6}M_\odot$ to $10^{-4}M_\odot$ depending on the models) from the proto-neutron star and map it onto the mesh of the hydro code. As for the latter case, we assume the mass and radius of proto-neutron star arbitrarily as inputs like the cases in QW. We solve the Oppenheimer-Volkoff equation to obtain the structure of a thin layer above the given radius. We assume the temperature and the electron fraction are constant in the whole layer and take $T = 3$ MeV and $Y_e = 0.25$ in the current study. For both cases, we have confirmed that the initial configuration settles into static state within a short time after remapping as long as we switch off the neutrino reactions.

We take as a reference the average energy of neutrinos as

$$\langle E_{\nu_e} \rangle = 10 \quad \text{MeV}, \tag{15}$$

$$\langle E_{\bar{\nu}_e} \rangle = 20 \quad \text{MeV}, \tag{16}$$

$$\langle E_{\nu_\mu} \rangle = 30 \quad \text{MeV}. \tag{17}$$

Similar values are chosen in the analytic studies (QW, Otsuki et al. 1999). The average energies of μ, τ neutrinos and anti-neutrinos are assumed to be identical. We give the neutrino luminosities as inputs and assume that they are constant during the simulations. We also assume that the luminosities are common to all flavors. These simple settings for neutrinos are meant to compare with previous studies and to clarify the dependence on the luminosity and average energy of neutrinos and the mass and radius of proto-neutron stars. In the forth-coming paper, we will take more realistic neutrino spectra from the proto-neutron star simulations taking into account energy distribution, flavor-dependence and time-dependence.

3 Numerical results

3.1 Models based on proto-neutron star cooling simulations

We start with a model based on the proto-neutron star cooling simulations with the baryon mass of $1.62 M_\odot$. As an initial configuration, we employ the output at $t = 3$ sec of the proto-neutron star cooling simulation. We set the neutrino luminosities $L_{\nu_i} = 1 \times 10^{51}$ ergs/s for each species. The total luminosity, therefore, amounts to $L_\nu^{tot} = 6 \times 10^{51}$ ergs/s. The outer boundary pressure is set to be $p_{out} = 10^{22}$ dyn/cm^2. We take the radius of the neutrinosphere as $R_\nu = 16.4$ km.

We display in Fig. 1 the trajectories of mass elements during the simulation. The positions in radius are shown as a function of time. The trajectories of every 5 mass shells are presented here. The surface layers are heated by neutrinos and escape from the surface of the proto-neutron star one by one, forming the neutrino-driven wind. Figure 2 depicts the temperatures of the mass elements as a function of time. The temperature once becomes as high as 3 MeV due to the neutrino-heating and cools down to 0.1 MeV during the expansion. The pressure of the material balances with the imposed outer pressure when the temperature of the material becomes around 0.1 MeV, which roughly corresponds to this pressure. Figure 3 shows the densities of the mass elements as a function of time. The density of the material in the wind decreases due to expansion and stays around 10^4 g/cm^3. The entropy per baryon, S, becomes high during the evolution and reaches up to 87 (in units of k_B hereafter) at $T = 0.5$ MeV in this model. After that, the entropy remains roughly constant because the heating and cooling processes become negligible.

We define the expansion time scale, τ_{dyn}, as the e-fold time of temperature at $T = 0.5$ MeV during the expansion. It is found to be 0.15 seconds in this model. This definition accords with those in the previous papers by Hoffman et al. (1997) and Otsuki et al. (1999) to discuss on the α-rich freeze-out and the r-process. The mass loss rate, $\dot{M}$, which is the amount of the ejected mass divided by the mass loss time, is found to be $1.5 \times 10^{-5} M_\odot$/s.

Figure 4 displays the time evolution of the electron fraction for one of the mass elements. The electron fraction is small at the beginning since the mass element was originally in the

surface layer of the proto-neutron star. It increases due to neutrino reactions on nucleons during the expansion in the wind and reaches 0.46 at $T = 0.5$ MeV. The equilibrium value of the electron fraction is roughly determined by the neutrino spectra. We will discuss this point in section 4.1.

To explore their dependences, we have performed simulations with different neutrino luminosities and simulations with a different proto-neutron star mass. For the latter case, we employ the profile of a more massive proto-neutron star at 3 seconds in the cooling simulation. Table 1 summarizes the model parameters and some results of the numerical simulations.

Figure 5 shows the dependence of the key quantities on the neutrino luminosity. For comparisons, we plot also the values obtained with the analytic treatment (Otsuki et al. 1999), in which the neutron star mass and the radius are assumed to be $1.4M_\odot$ and 10 km, respectively. The dependence on the neutrino luminosity is found qualitatively similar between the numerical simulations and the analytic treatment despite the difference of initial profile. We see, however, quantitative differences in the mass loss rate and the entropy per baryon. The mass loss rate in the current numerical study turns out larger than that in the analytic study while the entropy per baryon tends to be lower.

3.2 Models with given mass and radius

To compare with the analytic treatment in detail, we have performed the numerical simulations for the proto-neutron star with the mass and radius given by hand. This is meant to check the numerical results by the comparison with the analytic treatment for simple cases as well as to understand the results obtained in the previous section better.

Table 2 summarizes the model parameters and some results of the numerical simulations. We choose $1.4M_\odot$ and $2.0M_\odot$ for the mass and 10 km for the radius to compare with the results by Otsuki et al. (1999), where the general relativistic analytic study has been worked out for the same parameters.

Figure 6 shows the key quantities of the neutrino-driven wind as a function of neutrino luminosity both for the numerical simulations and the analytic treatment. The general trend of the luminosity dependence is common. As for the mass loss rate and the entropy per baryon,

the results of numerical simulations accord quantitatively well with those of analytic treatment. On the other hand, the expansion time scale is found systematically shorter in the numerical simulations than in the analytic study. The difference becomes large in some cases, which is preferable for r-process.

We have found that this difference of the expansion time scale mainly arises from our proper treatment of the equation of state. In the analytic studies done so far, they used the equation of state of the radiation-dominated matter

$$p = \frac{11\pi^2}{180} T^4. \tag{18}$$

even for temperatures below 0.5 MeV. It overestimates the pressure of electrons/positrons in the low temperature regimes. As a result, the pressure at large radii, where the temperature is low, is larger in the analytic treatment than in our simulations with the same temperature. The larger pressure results in a longer expansion time scale since it decelerates the wind.

We have investigated this issue in detail for model c01. In the numerical simulations, we impose a constant pressure (1×10^{22} dyn/cm^3 for model c01) at the outer boundary while in the analytic treatment the temperature is assumed to be 0.1 MeV at the radius 10^4 km. Although the temperatures at the radius 10^3 km are 0.12 MeV in both cases, the pressures there are found 2.2×10^{22} dyn/cm^2 in the analytic treatment and 1.1×10^{22} dyn/cm^2 in the simulation. This discrepancy comes from different treatments of the equation of state and the smaller pressure results in a shorter expansion time in the simulation. To confirm this interpretation, we recalculate the analytic model with the lower temperature (0.09 MeV) which gives the the same pressure at the radius 10^3 km as model c01. In this case, the profiles of the pressure become closer to each other, although the pressure in the analytic treatment is still higher inside the radius 10^3 km. The expansion time scale becomes shorter (0.10 sec) than the original analytic model (0.16 sec) and closer to the value (0.05 sec) in the simulation. Thus it is clear that the proper treatment of the equation of state is crucial to obtain the expansion time scale. We stress again that the shorter expansion time scale is preferable for r-process.

We have also examined the dependence on the pressure imposed at the outer boundary. When we take a smaller pressure (1×10^{20} dyn/cm^2) the expansion time scale becomes shorter (0.026 sec) than the value (0.05 sec) in the standard case (1×10^{22} dyn/cm^2), while the other

quantities such as the mass loss rate and the entropy per baryon change little. The temperature becomes as low as 0.04 MeV due to the rapid expansion, which roughly corresponds to the pressure imposed at the outer boundary. The radius and the density become larger and lower, correspondingly.

Here we comment on the effect of the general relativity. As pointed out by Cardall & Fuller (1997) and Otsuki et al. (1999), we found that the entropy per baryon is higher and the expansion time scale is shorter than the corresponding results in the Newtonian treatment by Qian & Woosley (1996).

4 R-process nucleosynthesis

4.1 Conditions for r-process

Based on the hydrodynamical simulations of the neutrino-driven wind, we discuss here key quantities for the r-process nucleosynthesis, that is, the entropy per baryon, expansion time scale and electron fraction at the time of the nucleosynthesis. Higher entropy per baryon, shorter expansion time scale and lower electron fraction (and their combinations) are favorable for the r-process nucleosynthesis (Hoffman et al. 1997; Meyer and Brown 1997).

Figure 7 summarizes all the results of the numerical simulations listed in Tables 1 and 2 in the plane of the expansion time scale and the entropy per baryon. The analytic models are also shown in the same figure. It is found that the results for the models based on the proto-neutron star cooling simulations are similar to the analytic model with $1.4M_{\odot}$. Among them, the more massive case with $2.00M_{\odot}$ is rather preferable for the r-process having higher entropy per baryon. As for the models with given mass and radius, they have higher entropy and shorter expansion time scale (upper left direction in the figure) than the models based on the proto-neutron star cooling simulations. This is mainly because the former has a smaller radius and a deeper gravitational potential than the latter (for details, see Qian & Woosley 1996). We can see here again the general trend that the more massive models are the better for the r-process. Using analytic model with general relativity, Otsuki et al. (1999) pointed out that the r-process might be possible for massive neutron stars with a short expansion time scale.

Our results with the numerical simulations show even shorter expansion time scale having a higher possibility of the successful r-process. Indeed, in the analytic study by Otsuki et al. (1999), the r-process is possible only for high luminosity cases, while the current study relaxes this constraint.

Another key quantity is the electron fraction. If the electron fraction is small enough, the r-process is possible even with low entropy per baryon and with long expansion time scale. The electron fraction in the neutrino-driven wind is governed by the neutrino captures on nucleons, thereby determined by the relative strength of the luminosities and energy spectra of the electron-type neutrinos and anti-neutrinos. In the model with a higher average energy for the electron-type anti-neutrinos, $\langle E_{\bar{\nu}_e} \rangle = 30$ MeV, the electron fraction at $T = 0.5$ MeV turns out to be 0.38 which is lower than 0.46 in model p06 with $\langle E_{\bar{\nu}_e} \rangle = 20$ MeV.

The electron fraction in the neutrino-driven wind can be estimated by the average energies of neutrinos and anti-neutrinos as

$$Y_e^{eq} = \frac{\langle E_{\nu_e} \rangle + 2\Delta}{\langle E_{\nu_e} \rangle + \langle E_{\bar{\nu}_e} \rangle}, \tag{19}$$

where Δ is the neutron-proton mass difference (Qian and Woosley 1996). Here we assume that the charge-changing neutrino capture reactions are in equilibrium and that the luminosity of neutrinos are the same as that of anti-neutrinos.

The electron fractions obtained in the numerical simulations roughly accord with the above estimation. We found that the neutrino capture reactions come to equilibrium before the temperature falls down to 0.5 MeV. When the temperature goes below 0.5 MeV, the mass fraction of α-particle becomes large and that of proton becomes negligible. In this situation, the electron fraction remains almost constant with only a slight increase due to the anti-neutrino capture on neutrons. The neutrino capture on protons has already frozen out due to the lack of free protons.

4.2 R-process network calculation

We have performed a nucleosynthesis calculation using a result of our hydrodynamical simulations for neutrino-driven winds in order to demonstrate that the r-process nucleosynthesis is indeed possible for the model.

We employ model b09 (the mass $2.0M_\odot$ and the radius 10 km with $L_\nu^{tot} = 6 \times 10^{52}$ ergs/s) which has the shortest expansion time scale among our models. We pick up one of mass trajectories in the hydrodynamical result and input it to the r-process calculation. We start the r-process calculation at the time when the temperature becomes $T_9 \equiv \frac{T}{10^9 \mathrm{K}} = 9$ in the trajectory. Figure 8 displays the temperature and density trajectories taken from the hydrodynamical simulation. The origin of time in the figure is shifted so that the temperature becomes $T_9 = 9$ there. In the network calculation, matter is assumed to be initially composed of neutrons and protons with the electron fraction $Y_e = 0.44$, the result of the hydrodynamical simulation.

The nuclear reaction network employed in the code covers neutron-rich nuclei from the β stability line to the neutron drip line for $Z = 10 \sim 100$. It includes also light nuclei which are required to synthesize seed elements for the r-process. The neutron capture, its reversed reaction, β decay and β delayed emission are incorporated for $Z \geq 10$. On top of the reactions for the r-process, charged particle reactions are included to follow the α-rich freeze-out. The (α, n) reactions up to $Z = 36$ and (α, γ) reactions up to ^{28}Si are included. The α reactions that produce ^{9}Be, ^{12}C and beyond are also included. The details of the reaction network code will be described elsewhere (Terasawa et al. 1999).

The neutron-to-seed ratio at $T_9 = 2.5$ is found to be 120 in the r-process network calculation. The electron fraction at the same temperature is 0.42. The rapid expansion during the time of the α-rich freeze out ($T \sim 0.5$ MeV) leads to only a small amount of the seed elements resulting in the high neutron-to-seed ratio. With this high neutron-to-seed ratio, the r-process elements up to $A \sim 200$ are produced ensuingly. Figure 9 shows the yields of our r-process network calculation. It is remarkable that the 3rd peak at $A = 195$ as well as the 2nd peak at $A = 130$ is reproduced appropriately. It is emphasized that this result is consequence of the short expansion time scale and accords with the result shown by Otsuki et al. (1999). The shorter expansion time scale obtained in the current simulation than in the analytic treatment further enhances the 3rd peak height having a higher neutron-to-seed ratio.

5 Summary

We study numerically the general relativistic hydrodynamics of the neutrino-driven wind blown from the proto-neutron stars and examine the r-process nucleosynthesis there. We focus on the entropy per baryon, electron fraction, expansion time scale and mass loss rate as key quantities for the r-process. By employing the results of the proto-neutron star cooling simulations as inputs for the neutrino-driven wind simulations, we investigate those quantities in realistic situations. We also make comparison with the results of analytic treatment by assuming masses and radii of proto-neutron stars as in the analytic study. We explore the dependence on the profile of the proto-neutron star as well as neutrino luminosity.

We find that the entropy per baryon and the expansion time scale are neither high nor short enough for the r-process in the models based on proto-neutron star cooling simulations. This is mainly because the radius of the proto-neutron star is rather large due to the thermal pressure. The expansion time scale has a strong dependence on the neutrino luminosity and it becomes as short as 10 msec for high neutrino luminosities, which is close to the value required in the rapid expansion scenario by Otsuki et al. (1999).

On the other hand, the hydrodynamical simulations for models with given mass and radius show that larger masses and smaller radii are found more favorable for the r-process. In the case of massive and compact neutron stars with high neutrino luminosities, the entropy per baryon is high enough and the expansion time scale is short enough. We demonstrate by the network calculation a successful r-process nucleosynthesis for a model of our hydrodynamical simulations. The 2nd and 3rd abundance peaks of r-process elements and their relative height are well reproduced.

We find that the expansion time scales obtained in the simulations are systematically shorter than the values in the analytic treatment. This is because the pressure at low temperature is overestimated in the analytic treatment, and therefore the expansion time scale becomes longer than what one expects with the proper treatment of the equation of state as in our study. Since the expansion time scale determines the neutron-to-seed ratio crucially, even a small decrease in the time scale may increase the neutron-to-seed ratio substantially making ensuing r-process more promising.

We notice here that the dynamics of the neutrino-driven wind is sensitive to the outer boundary condition. A decrease of the outer boundary pressure results in a shorter expansion time scale. On the other hand, the temperature should remain around 0.1 MeV for about 1 second so that the r-process could occur. If the outer boundary pressure is too small, the temperature decreases too rapidly for the r-process to proceed even though the expansion time scale is short enough for the high neutron-to-seed ratio. So far most of the previous studies adopted $T = 0.1$ MeV at 10^4 km as a boundary condition, however, we have to bare in mind this additional uncertainty.

The fact that the results of hydrodynamical simulations based on the proto-neutron star cooling simulation turns out not suitable for the r-process does not exclude the possibility of the r-process in the neutrino-driven wind. We have assumed the neutrino luminosity is constant in time in the current study. This is too simple an assumption. In reality, however, the neutrino luminosity decreases with time scale of 10 seconds and one should not forget the time dependence of the luminosity. In the simulation of Woosley et al. (1994), the r-process takes place in a late stage with a high entropy when the neutrino luminosity is low and the outer material is already expanding due to the high neutrino luminosity in the earlier stage. The numerical simulations with the time dependent luminosities as well as realistic neutrino energy spectra are in progress and will be reported elsewhere.

Acknowledgment

We are grateful to S. Wanajo, T. Kajino and I. Tanihata for encouraging comments and fruitful discussions on the r-process nucleosynthesis. We would appreciate K. Oyamatsu, H. Shen and H. Toki for the advice on the usage of the relativistic EOS table. K. S. would like to express special thanks to H. Shen for providing the numerical code for the EOS with α-particles. The numerical simulations have been performed on the supercomputer VPP700E/128 at RIKEN and VPP500/80 at KEK (KEK Supercomputer Projects No.98-35 and No.99-52). This work is partially supported by the Grants-in-Aid for the Center-of-Excellence (COE) Research of the ministry of Education, Science, Sports and Culture of Japan to RESCEU (No.07CE2002).

References

Burbidge, E.M., Burbidge, G.R., Fowler, W.A. and Hoyle, F. 1957, Rev. Mod. Phys. 29, 547

Cardall, C.Y. and Fuller, G.M. 1997, ApJ 486, L111

Cowan, J.J., Thielemann, F.-K. and Truran, J.W. 1991, Phys. Rep. 208, 267

Duncan, R.C., Shapiro, S.L. and Wasserman I. 1986, ApJ 309, 141

Hillebrandt, W. 1978, Space Sci. Rev. 21, 639

Hoffman, R.D., Woosley, S.E. and Qian, Y.-Z. 1997, ApJ 482, 951

Käppeler, F., Beer, H. and Wisshak, K. 1989, Rep. Prog. Phys. 52, 945

Meyer, B.S., Mathews, G.J., Howard, W.M., Woosley, S.E. and Hoffman, R.D. 1992, ApJ 399, 656

Meyer, B.S. and Brown, J.S. 1997, ApJS 112, 199

Otsuki, K. 1999, Ph.D Thesis, Osaka University

Otsuki, K., Tagoshi, H., Kajino, T. and Wanajo, S. 2000, ApJ 531, in press

Qian, Y.-Z. and Woosley, S.E. 1996, ApJ 471, 331 (QW)

Shen, H., Toki, H., Oyamatsu, K. and Sumiyoshi, K. 1998, Nucl. Phys. A637, 435

Shen, H., Toki, H., Oyamatsu, K. and Sumiyoshi, K. 1998, Prog. Theor. Phys. 100, 1013

Sneden, C., McWilliam, A., Preston, G.W., Cowan, J.J., Burris, D.I. and Armosky, B.J. 1996, ApJ 467, 819

Sumiyoshi, K., Kuwabara, H. and Toki, H. 1995, Nucl. Phys. A581, 725

Sumiyoshi, K., Suzuki, H. and Toki, H. 1995, A&A 303, 475

Sugahara, Y. and Toki, H. 1994, Nucl. Phys. A579, 557

Suzuki, H. 1994, Physics and Astrophysics of Neutrinos, edited by Fukugita, M. and Suzuki, A., (Springer-Verlag, Tokyo, 1994), p763

Takahashi, K., Witti, J. and Janka, H.-Th. 1994, A&A 286, 857

Terasawa, M., Sumiyoshi, K., Tanihata, I. and Kajino, T., in preparation

Witti, J., Janka, H.-Th. and Takahashi, K. 1994, A&A 286, 841

Woosley, S.E., Wilson, J.R., Mathews, G.J., Hoffman, R.D. and Meyer, B.S. 1994, ApJ 433, 229

Yamada, S. 1997, ApJ 475, 720

Yamada, S., Janka, H.-Th. and Suzuki, H. 1999, A&A 344, 533

Table caption

Table 1 Summary of models based on proto-neutron star cooling simulations. M_B, M_G and R are the baryon mass, gravitational mass and radius of the proto-neutron star. For the definition of the other entries, see the text.

Table 2 Summary of models with given mass and radius. M_G and R are gravitational mass and radius of the proto-neutron star. For the definition of the other entries, see the text.

Table 1

Model	M_B $[M_\odot]$	M_G $[M_\odot]$	R [km]	L_ν^{tot} [ergs/s]	S $[k_B]$	τ_{dyn} [sec]	$\dot{M}$ $[M_\odot/\mathrm{s}]$	Y_e
p07	1.62	1.55	17.7	3.6×10^{51}	100	3.2×10^{-1}	6.1×10^{-6}	0.47
p06	1.62	1.55	17.7	6.0×10^{51}	87	1.5×10^{-1}	1.5×10^{-5}	0.46
p08	1.62	1.55	17.7	1.8×10^{52}	76	5.3×10^{-2}	1.0×10^{-4}	0.45
p09	1.62	1.55	17.7	6.0×10^{52}	65	1.6×10^{-2}	8.6×10^{-4}	0.44
r06	2.00	1.88	16.9	3.6×10^{51}	128	2.9×10^{-1}	3.4×10^{-6}	0.46
r03	2.00	1.88	16.9	6.0×10^{51}	119	1.5×10^{-1}	8.3×10^{-6}	0.46
r12	2.00	1.88	16.9	1.8×10^{52}	105	5.0×10^{-2}	5.6×10^{-5}	0.45
r01	2.00	1.88	16.9	6.0×10^{52}	84	1.5×10^{-2}	4.7×10^{-4}	0.44

Table 2

Model	M_G $[M_\odot]$	R [km]	L_ν^{tot} [ergs/s]	S $[k_B]$	τ_{dyn} [sec]	$\dot{M}$ $[M_\odot/\mathrm{s}]$	Y_e
c02	1.40	10.0	3.6×10^{51}	142	9.7×10^{-2}	2.7×10^{-6}	0.46
c01	1.40	10.0	6.0×10^{51}	131	5.0×10^{-2}	6.5×10^{-6}	0.45
c08	1.40	10.0	1.8×10^{52}	121	1.2×10^{-2}	4.4×10^{-5}	0.44
c04	1.40	10.0	6.0×10^{52}	95	6.2×10^{-3}	4.2×10^{-4}	0.44
b17	2.00	10.0	3.6×10^{51}	263	1.0×10^{-1}	8.8×10^{-7}	0.46
b10	2.00	10.0	6.0×10^{51}	239	5.3×10^{-2}	2.2×10^{-6}	0.45
b18	2.00	10.0	1.8×10^{52}	196	9.6×10^{-3}	1.6×10^{-5}	0.44
b09	2.00	10.0	6.0×10^{52}	165	5.1×10^{-3}	1.3×10^{-4}	0.44

Figure captions

Figure 1 The trajectories of the mass elements in the neutrino-driven wind for model c01 as a function of time. Every 5 mass shells are shown here.

Figure 2 The temperatures of mass elements for the same model as Fig. 1.

Figure 3 The densities of mass elements for the same model as Fig. 1.

Figure 4 The electron fraction of a mass element for the same model as Fig. 1.

Figure 5 The luminosity dependence of the mass loss rate, entropy per baryon and expansion time scale for the models based on the proto-neutron star cooling simulations (symbols) and for the case of the analytic treatment (solid line). The solid circles are models with the baryon mass of $1.62M_\odot$ and the solid squares with the baryon mass of $2.00M_\odot$. The result of the analytic treatment is for the case with the gravitational mass of $1.4M_\odot$ and the radius of 10 km.

Figure 6 The luminosity dependence of the mass loss rate, entropy per baryon and expansion time scale for the models with given mass and radius (symbols) and for the analytic treatment (solid line). The open circles are models with the gravitational mass of $1.4M_\odot$ and the open squares with the gravitational mass of $2.0M_\odot$. The solid and dashed lines show the results of the analytic treatment with the gravitational mass of $1.4M_\odot$ and $2.0M_\odot$, respectively. The radii are taken as 10 km in all cases.

Figure 7 The expansion time scale (τ_{dyn}) and entropy per baryon (S) at the temperature $T = 0.5$ MeV. The solid circle and solid square symbols are for the models based on the proto-neutron star cooling simulations with the baryon mass of $1.62M_\odot$ and $2.00M_\odot$, respectively. The open circle and open square symbols are for the models with given mass and radius (the gravitational mass of $1.4M_\odot$ and $2.0M_\odot$, respectively). The solid and dashed lines show the results of the analytic treatment with the gravitational mass of $1.4M_\odot$ and $2.0M_\odot$, respectively. The radii are taken as 10 km in all cases.

Figure 8 The time evolution of the temperature and density of a mass element taken from

the model with the shortest expansion time scale (the gravitational mass of $2.0M_{\odot}$, the radius of 10 km, and the total neutrino luminosity of 6×10^{52} ergs/s). The time when the temperature becomes $T_9 = 9$ is defined to be 0.

Figure 9 The abundance of the r-process elements obtained by the network calculation using the trajectory shown in Fig. 8. The scaled r-process abundances from Käppeler, Beer and Wisshak (1989) are shown by dots for comparison.

Figure 1

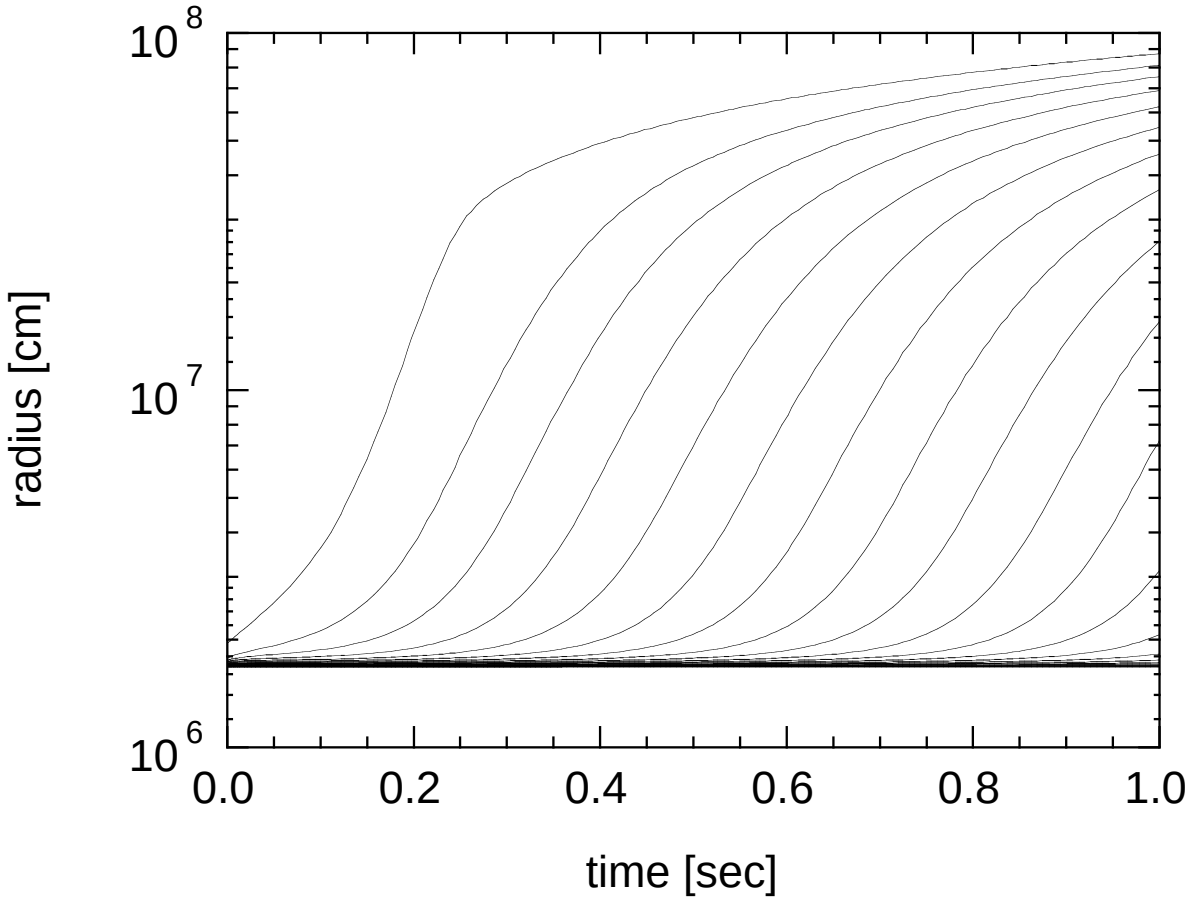

Figure 2

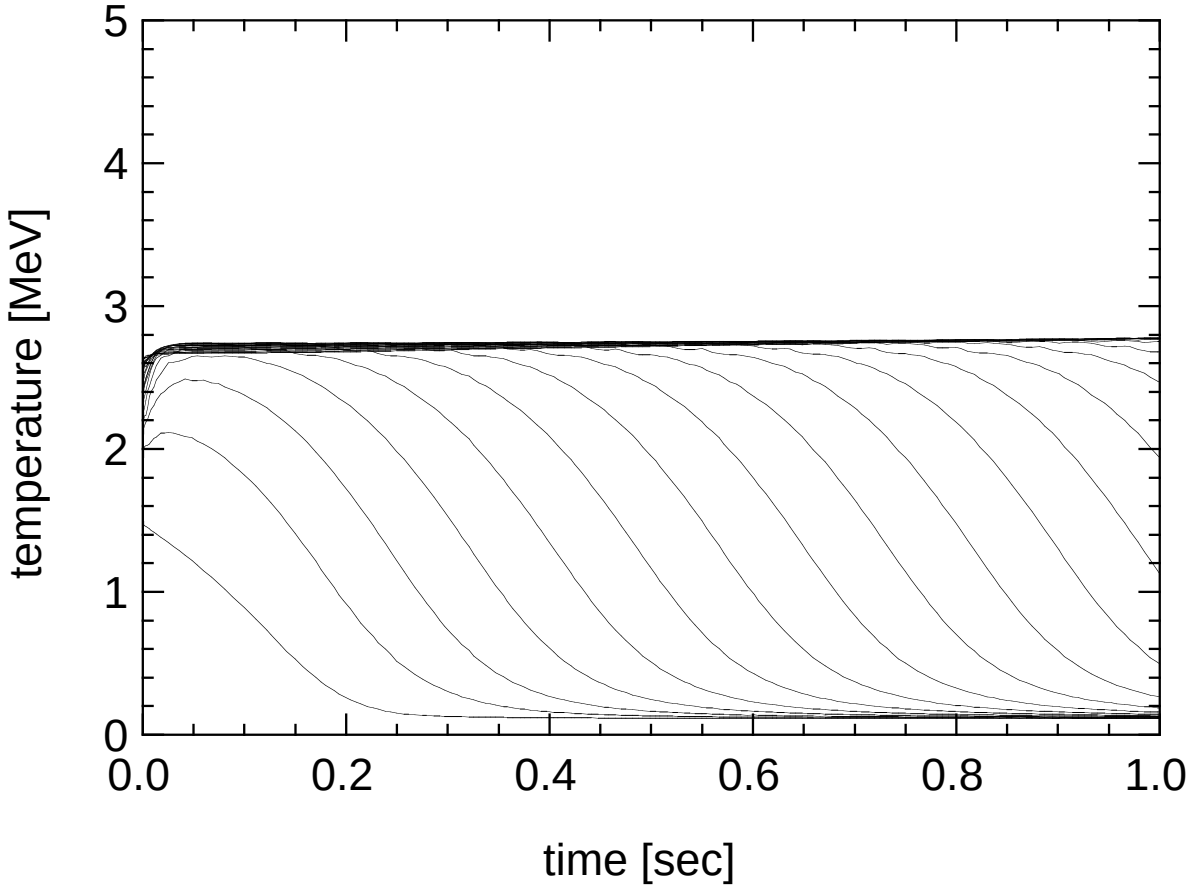

Figure 3

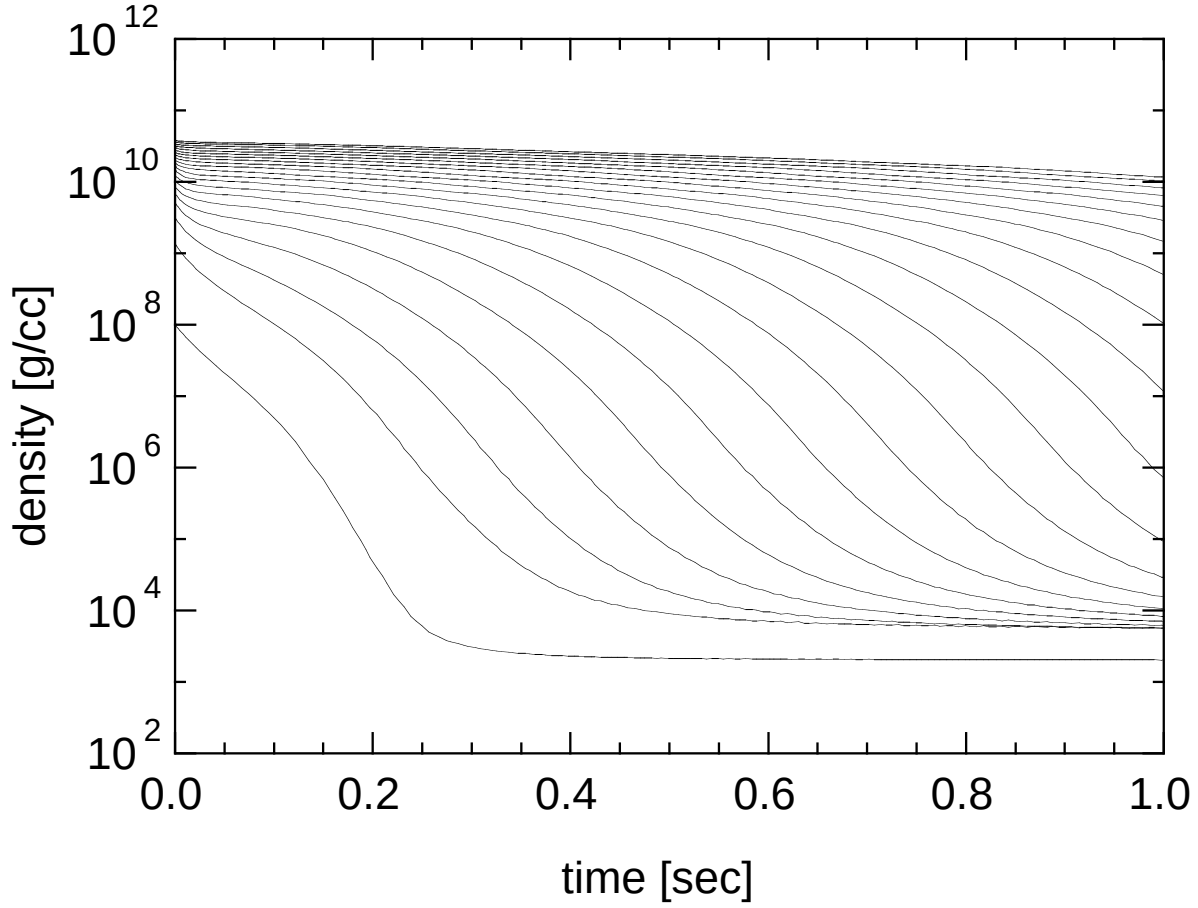

Figure 4

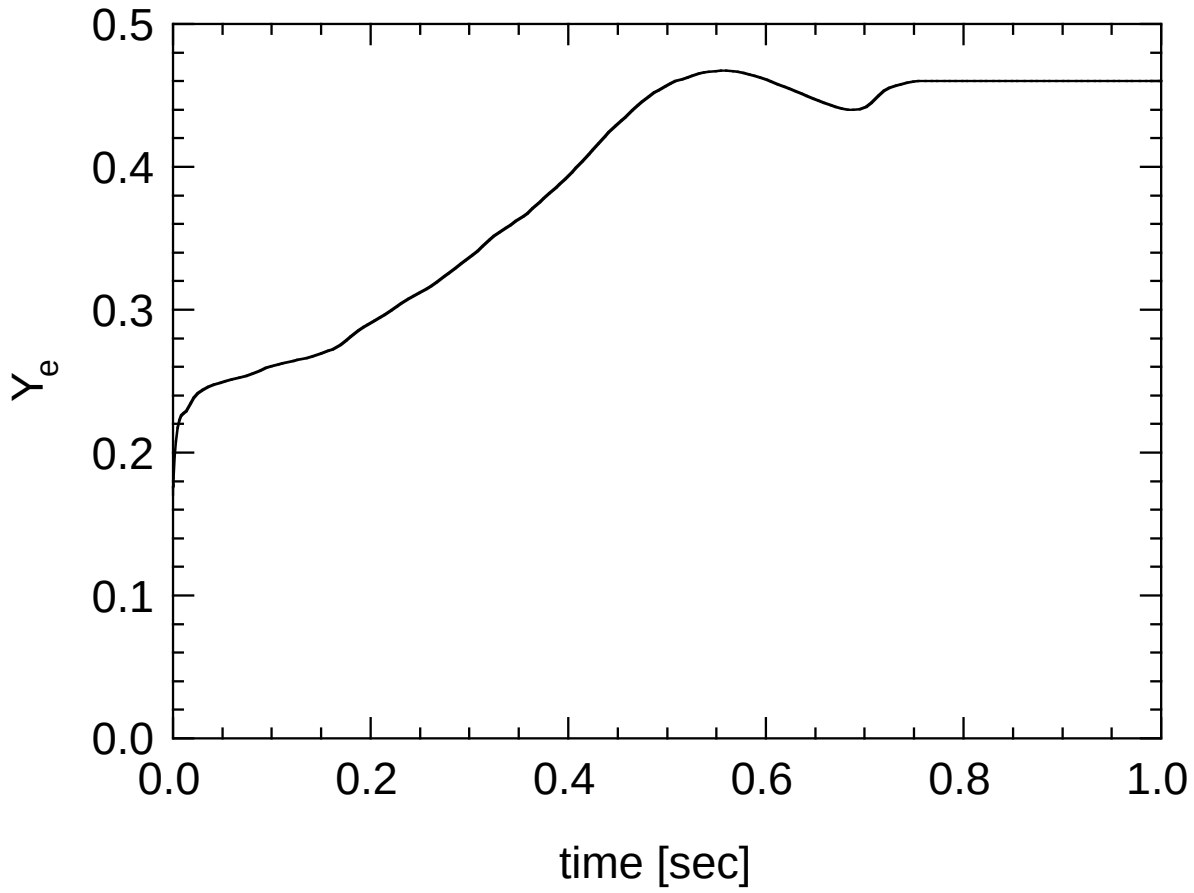

Figure 5

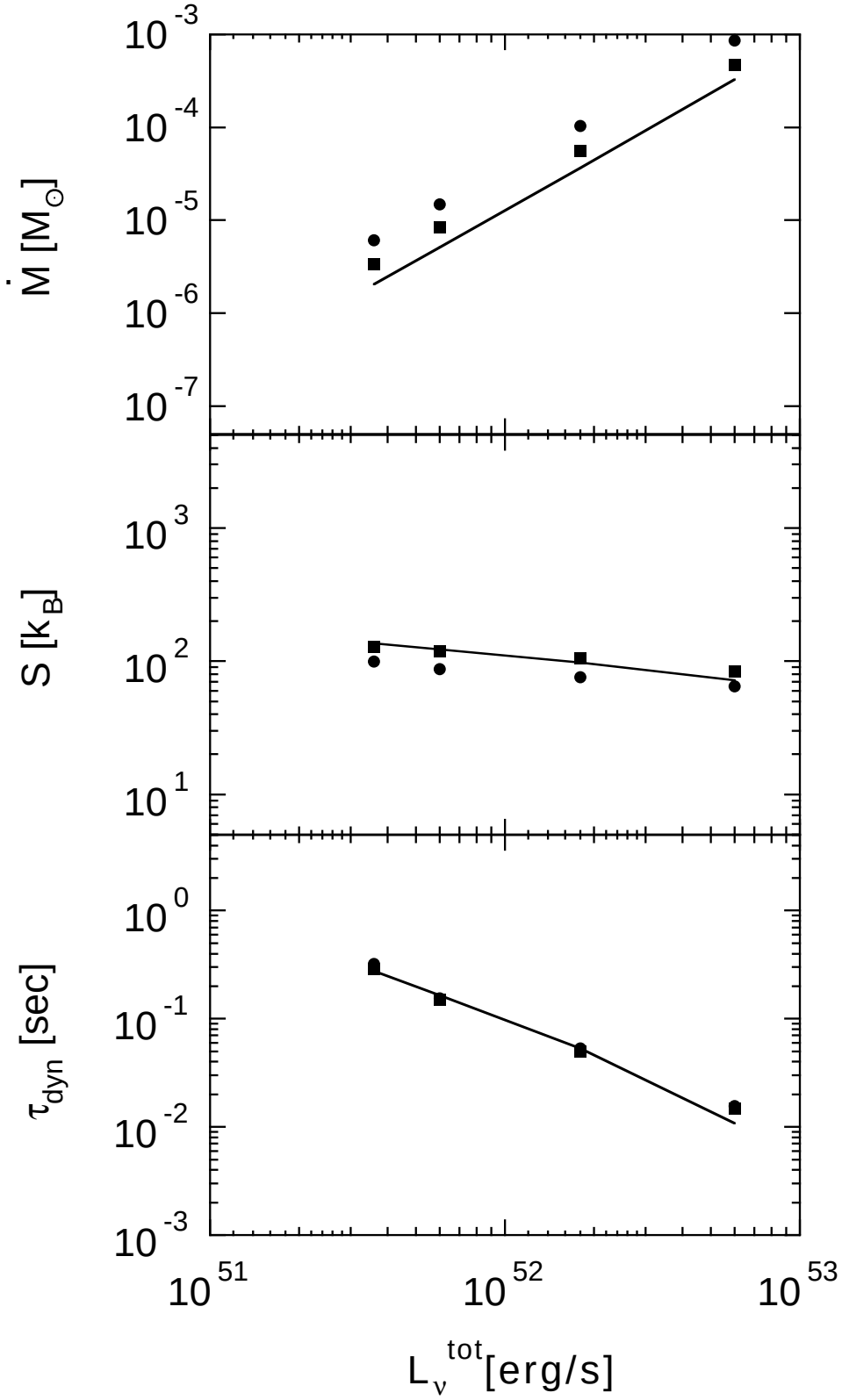
10^{-3}
10^{-4}
10^{-5}
10^{-6}
10^{-7}
$\dot{M}$ [$M_\odot$]
10^{3}
10^{2}
10^{1}
S [k_B]
10^{0}
10^{-1}
10^{-2}
10^{-3}
τ_{dyn} [sec]
10^{51}
10^{52}
10^{53}
L_ν^{tot}[erg/s]

Figure 6

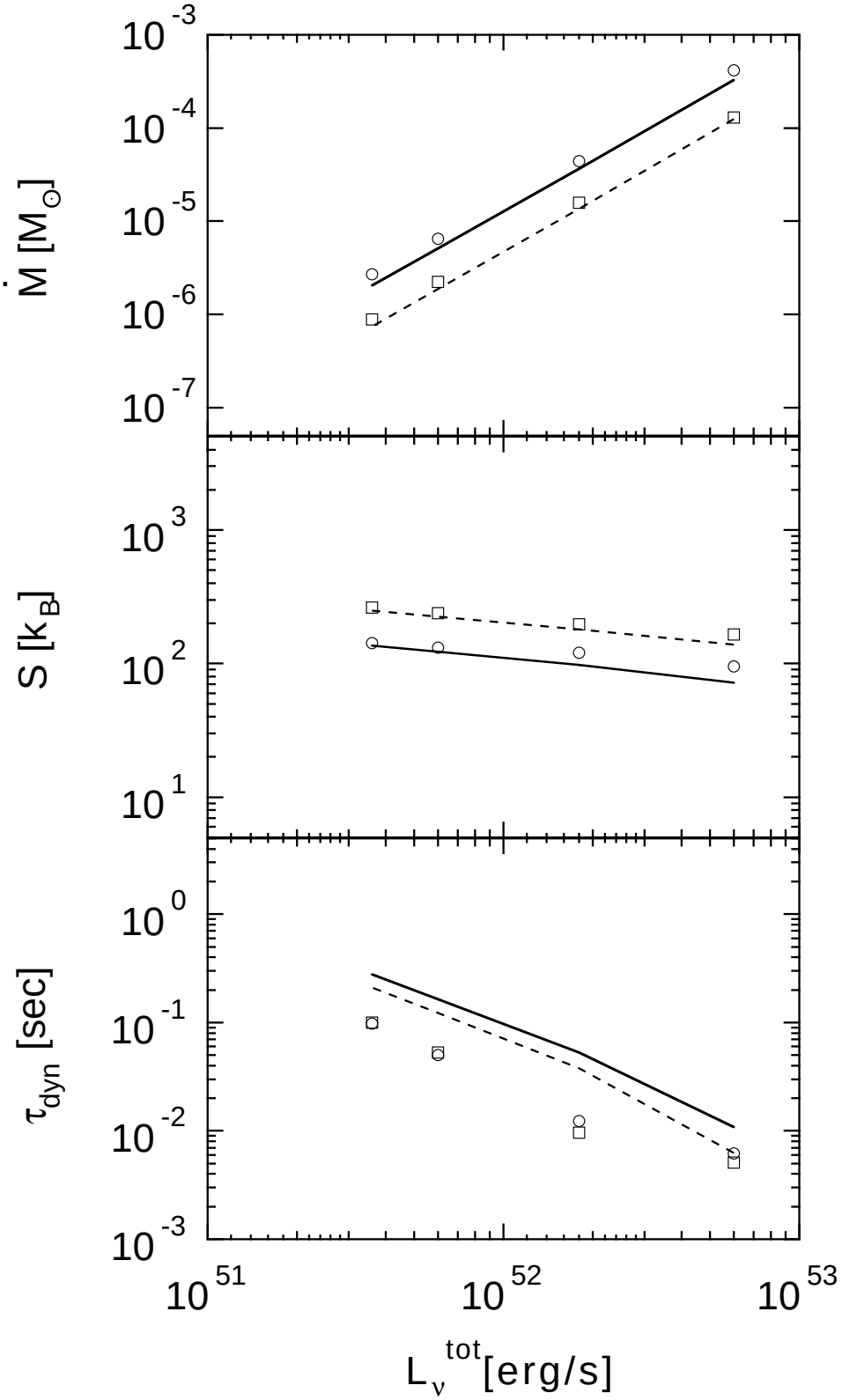
10^{-3}
10^{-4}
10^{-5}
10^{-6}
10^{-7}
$\dot{M}$ [$M_\odot$]
10^{3}
10^{2}
10^{1}
S [k_B]
10^{0}
10^{-1}
10^{-2}
10^{-3}
τ_{dyn} [sec]
10^{51}
10^{52}
10^{53}
L_ν^{tot} [erg/s]

Figure 7

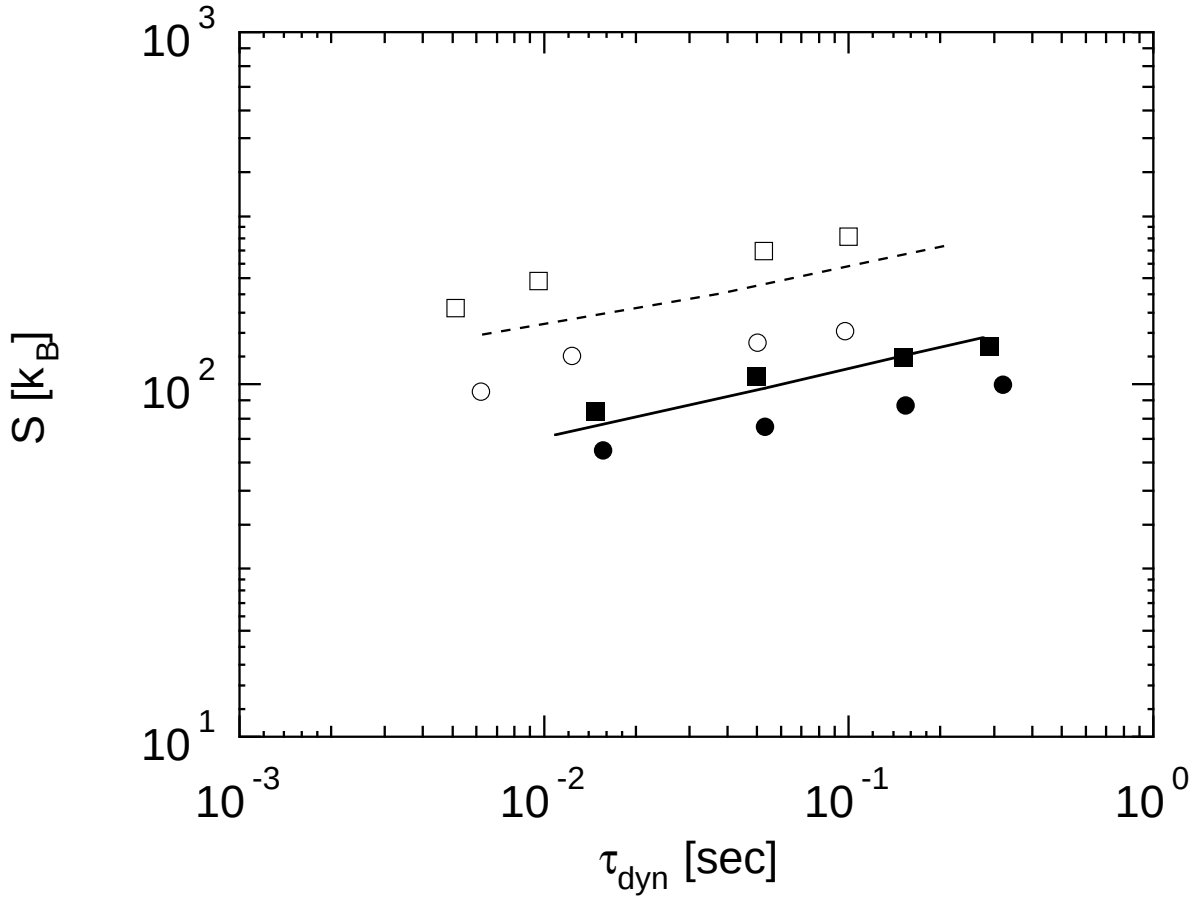

Figure 8

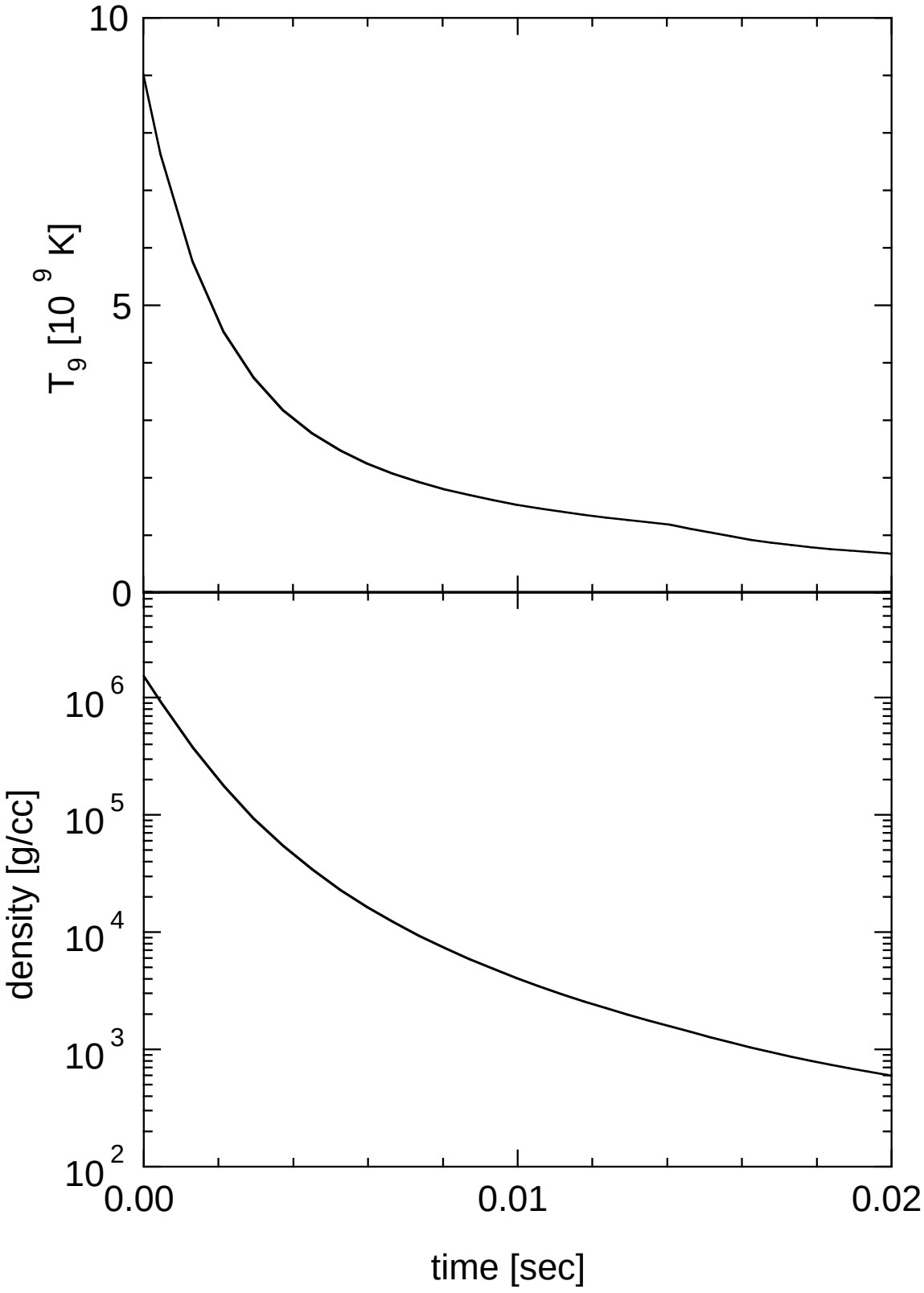
10
5
0
T_9 [10^9 K]
10^6
10^5
10^4
10^3
10^2
density [g/cc]
0.00
0.01
0.02
time [sec]

Figure 9